

Beamlines

J. Synchrotron Rad. (1998), **5**, 485–487

First results from the crystal structure analysis beamline at SPring-8

Yukio Noda,^{a*} Ken-ichi Ohshima,^b Hideo Toraya,^c Kiyooki Tanaka,^d Hikaru Terauchi,^e Hiroshi Maeta^f and Hiroyuki Konishi^g

^aFaculty of Science, Chiba University, Yayoi, Inage, Chiba 263, Japan, ^bInstitute of Applied Physics, University of Tsukuba, Tsukuba 305, Japan, ^cCeramic Research Laboratory, Nagoya Institute of Technology, Tajimi 507, Japan, ^dNagoya Institute of Technology, Showaku, Nagoya 466, Japan, ^eSchool of Science, Kwansai Gakuin University, Uegahara, Nishinomiyama 662, Japan, ^fDepartment of Materials Science and Engineering, JAERI, Tokai, Ibaraki 319-11, Japan, and ^gJAERI SPring-8, Kamigori, Ako, Hyogo 678-12, Japan. E-mail: ynoda@science.s.chiba-u.ac.jp

(Received 4 August 1997; accepted 22 October 1997)

Results from the first measurements at the crystal structure analysis beamline (BL02B1) at SPring-8 are presented. The capabilities of this beamline are also discussed.

Keywords: instrumental; SPring-8; BL02B1; crystal structure analysis.

1. Design and capabilities of the apparatus

The crystal structure analysis beamline (BL02B1) at SPring-8 was constructed through the collaboration of four subgroups: the Structural Phase Transition group, the Highly Precise Molecular Crystallography group, the Diffuse Scattering group and the High-Resolution Powder group. The central feature of this beamline is a specially designed seven-axis diffractometer (Noda *et al.*, 1996). The diffractometer is very similar to a conventional six-axis diffractometer, commonly used at beamlines of many synchrotron radiation facilities. One extra fast-scanning 2θ axis is added to the diffractometer in our system for conventional structure analysis. An off-centre-type χ -cradle is installed to mount accessories. Various types of apparatus, such as two different types of cryostat, a furnace, a vacuum camera, a Weissenberg camera, a diamond anvil cell, a Soller slit, spindles for powder samples on the φ axis *etc.*, can be attached in order to satisfy the wide range of interests of the four subgroups.

The seven axes, defined as 2θ (long), 2θ (short), ω , χ , φ , ω_A and $2\theta_A$, of the diffractometer are remotely controllable. Here, the subscript *A* denotes an analyser axis. We have two sets of ω_A and $2\theta_A$ axes, one of the typical configuration and a second set designed to measure the polarization of the scattered X-ray beam. The diffractometer is mounted on a base table, which facilitates precise placement of the sample crystal and incident collimator in the incident X-ray beam path. Four motorized motions are available in the base table: R_B , ω_B , X_B and Z_B . Here, R_B is a tilt, ω_B is a rotation, and X_B and Z_B are the translations of the base table. In Table 1, the minimum interval of angle or

Table 1

Minimum angle or stroke increment for one motor pulse, the scan speed per minute and the range of the movement for each axis of the seven-axis diffractometer and the base table.

All units are degrees, except for X_B and Z_B .

	Minimum increment	Speed	Range
2θ (long)	1×10^{-4}	120	–48 to +204
2θ (short)	4×10^{-4}	300	–58 to +201
ω	1×10^{-4}	120	–180 to +180
χ	2×10^{-4}	240	–180 to +180
φ	1×10^{-4}	120	–180 to +180
ω_{A1}	1×10^{-4}	180	–180 to +180
$2\theta_{A1}$	1×10^{-4}	180	–180 to +180
ω_{A2}	1×10^{-4}	180	–180 to +180
$2\theta_{A2}$	1×10^{-4}	180	–180 to +180
R_B	2.2×10^{-4}	5	–2 to +2
ω_B	5.72×10^{-5}	3.3	–2.5 to +3.0
X_B	4×10^{-4} mm	93	–37 to +63 mm
Z_B	1×10^{-4} mm	25	0 to 210 mm

stroke increment for one motor pulse, the scan speed and the range of motion for each axis are tabulated.

On the 2θ (long) axis a long counter arm with an analyser crystal is employed. We use this counter arm for high-resolution experiments. In addition, we can attach a high-precision Soller slit on the analyser crystal table for powder diffraction experiments. The Soller slit is designed so that the divergence is 0.03° , the transparency is 70% and the acceptance size is 20×15 mm. The long counter arm is also used for the measurement of precise lattice parameters in back-scattering geometry.

Other detection options are available using photographic methods. An image-plate system can be mounted on the long counter arm, and oscillation and Weissenberg photographs can be taken between 10 and 1000 K and up to 10 GPa. The camera radius is 250 mm and the size of the image plate is 440×260 mm. A fan-shaped Soller slit is also attached on the camera to remove background scatter from the cryostat Be windows. Two-dimensional detection is very useful in determining symmetry changes under extreme conditions, such as low temperature and high pressure. The prototype of our Weissenberg camera has already been described in the literature (Kuroiwa *et al.*, 1995).

A vacuum chamber, within which an image plate is attached, has also been prepared for structure analysis of very small crystals ($\sim 10 \mu\text{m}$). The camera radius is 75 mm and the size of the image plate is 440×260 mm. It covers $\pm 168^\circ$ for 2θ and $+65$ to -52° in the vertical direction. Since there are many materials whose structures are still unknown due to the difficulty of growing large crystals, this apparatus will open a new window for structure analysis.

We will provide two cryostats: one for structure analysis experiments, with a half-sphere Be window, and the other for larger (1 mm) crystals and powder pellets, with a cylindrical Be window. A diamond anvil cell can be installed in the latter cryostat. The temperature range achieved is 10–300 K. For the high-temperature region we will provide an electrical furnace, with a range of 300–1000 K. Some powder experiments require different sample attachments. For one such purpose, spindle plates can be attached on a goniometer head for a sample rotation rate of 2 Hz.

Synchrotron radiation from a bending magnet is monochromated by a standard SPring-8 monochromator. Double Si crystals are used in the monochromator and two mirrors are installed, upstream and downstream of the monochromator. An energy range of 5–90 keV will be available.

2. Results of the first experiments

We performed some first experiments to test the diffractometer and other options for five days just before the summer shutdown in 1997. The ring current during the experiments was either 18 or 1 mA. An Si 311 monochromator was used. The following results were obtained in these first experiments.

2.1. XAFS measurements

In order to test the ionization chambers and the communication between the monochromator and the computer systems we recorded XAFS patterns of Ag and Sn metal foils. The ring current was 18 mA. The absorption coefficient of Ag is shown in Fig. 1 as a function of energy. The XAFS pattern seems good, even around fairly high energies such as 25 and 30 keV. We evaluated the accuracy of the monochromated energy. The monochromator gives an accurate energy, within 30–50 eV. At the

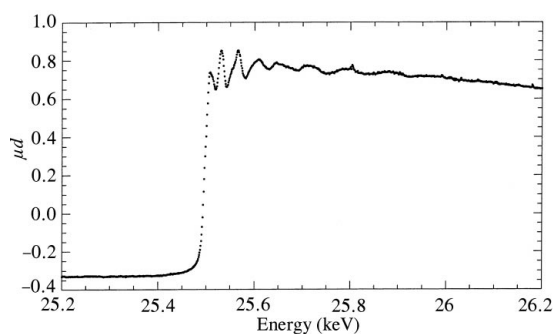


Figure 1
XAFS signal of Ag.

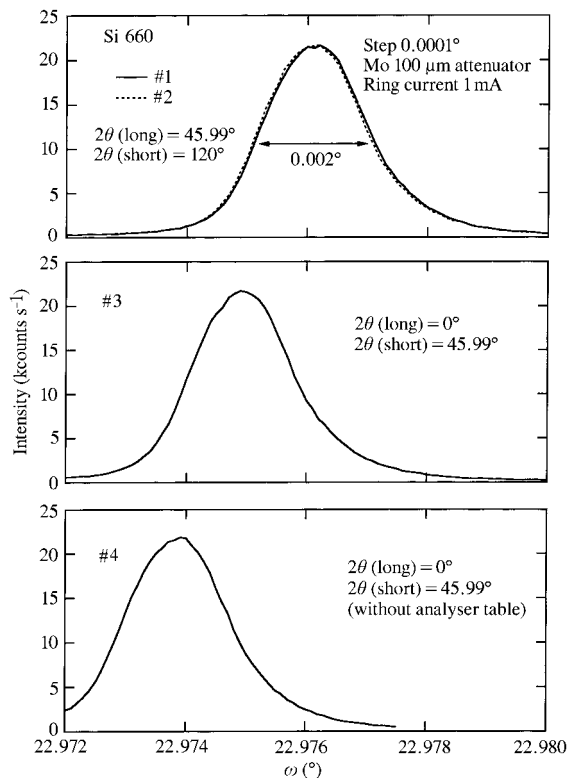


Figure 2
Si 660 rocking curves for different weight-balance conditions.

present time the actual energy is slightly higher than that requested.

2.2. Si single crystal

A diffraction pattern from an Si single crystal was taken to test the accuracy and the reproducibility of the diffractometer. Reflections from 220 to 10 10 0 were taken with 0.0001° minimum angle increment of the ω axis. As one example, the rocking curve of the 660 reflection is shown in Fig. 2. The data were taken when the ring current was 1 mA, and we used a 1/20 attenuator to reduce the intensity. The observed width was 0.002° FWHM. Runs #1 and #2 in the figure were taken to test the reproducibility

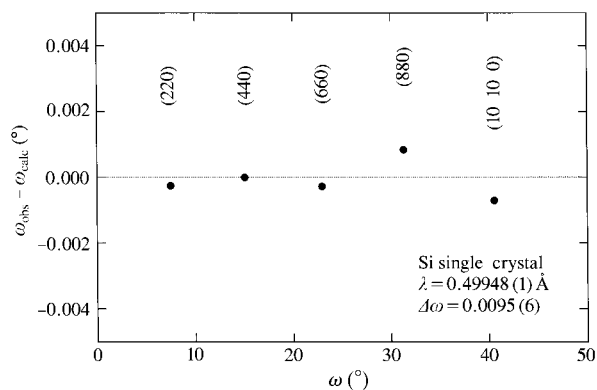


Figure 3
The differences between observed and calculated peak positions of Si $hh0$ reflections.

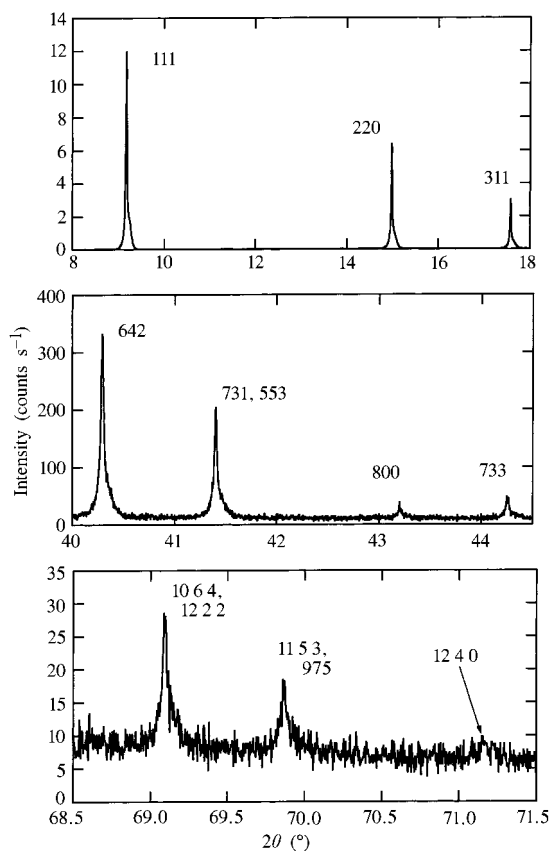


Figure 4
Powder diffraction profiles of Si.

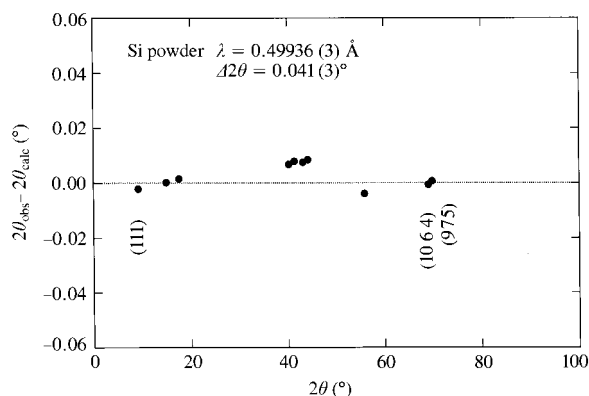


Figure 5
The differences between observed and calculated peak positions for Si powder reflections.

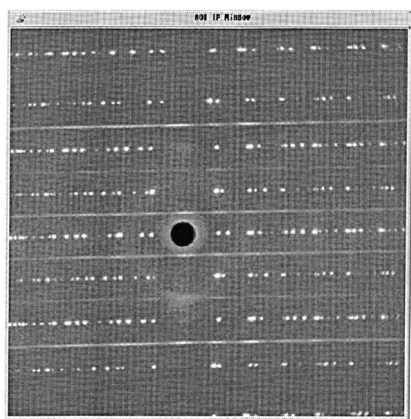


Figure 6
An oscillation photograph of $[\text{Ni}(\text{C}_6\text{H}_{14}\text{N}_2)_2][\text{PtBr}_2(\text{C}_6\text{H}_{14}\text{N}_2)_2]\text{Br}_4$ taken using the vacuum camera.

under identical conditions of the diffractometer. The obtained diffraction pattern was well reproduced and the accuracy seems to be within 0.0002° . Recall that there are two counter systems in the diffractometer, the long-arm counter and the short-arm counter. The above data were taken with the long-arm counter, while the short-arm counter was positioned at 120° . We changed the counter arms so that the short-arm counter was positioned at the diffraction angle while the long-arm counter was left at 0° . This configuration changes the weight balance in the diffractometer. The result is given in Fig. 2 as run #3. The peak position shifts 0.001° , but the width does not change. Further, we removed the analyser table from the long-arm counter to test the effect of this weight balance; the result is given as run #4. The peak position moves an additional 0.001° .

We calculated the wavelength of the incident X-rays by using the known lattice constant of the silicon sample. The result was $0.49948(1) \text{ \AA}$ for a requested setting of 0.50000 \AA . This value is consistent with the result of the XAFS measurements. In Fig. 3 we show the difference between the observed and the calculated peak positions. The consistency is satisfactory and the differences are within 0.0005° .

2.3. Si powder sample

First we tested the Soller slit for powder diffraction by comparing it with a conventional blade-type slit. As expected, the

width of the Si 111 peak observed with the Soller slit is much less than that observed with a blade-type slit, by a factor of three, to give the same peak intensity. We used a 2 mm-diameter incident beam; the advantage of the Soller slit will increase when we use a wide incident beam which matches the acceptance size (20 mm) of the Soller slit.

We took several Si powder reflections, up to 13 7 1, when the ring current was 18 mA. In Fig. 4, powder diffraction profiles of Si are shown. The widths observed are 0.04° for all peaks. In Fig. 5 we show the difference between the observed and the calculated peak positions. The consistency is satisfactory and the differences are within 0.005° . Again we calculated the wavelength of the incident X-rays by using the known lattice constant of the silicon sample. The result was $0.49936(3) \text{ \AA}$, and this value is essentially consistent with the result of the XAFS measurements and the Si single-crystal experiments.

2.4. Vacuum camera

We tested the vacuum camera with several crystals to evaluate its capabilities. The ring current was 18 mA and the wavelength was set to 0.5 \AA . First we took a photograph of an SrTiO_3 crystal whose size was 1.5 mm. For a crystal of this size, diffraction spots were seen up to a diffraction angle of 170° , but there was a large scattered background coming from the crystal itself. Next we took a photograph using a metal-organic crystal, $[\text{Ni}(\text{C}_6\text{H}_{14}\text{N}_2)_2][\text{PtBr}_2(\text{C}_6\text{H}_{14}\text{N}_2)_2]\text{Br}_4$, which is characterized by a Pt–Ni chain structure. The crystal size was $0.3 \times 0.1 \times 0.05 \text{ mm}$. In Fig. 6, the oscillation photograph is shown, in which the central part of the imaging plate around 20° is enlarged. The rotation angle was 10° and the exposure time was 20 min. The diffraction spots are clearly seen. The diffuse lines are also seen, which originate from the disordered character of the Pt–Ni chains. Finally, we took a photograph of a KNiF_3 crystal, whose size was $58 \mu\text{m}$, when the ring current was 1 mA. We could see diffraction spots so we consider that a structure analysis with a $10 \mu\text{m}$ crystal should be possible if the ring current is increased to 100 mA and focusing of the beam by the monochromator and mirrors is realised.

3. Summary

We constructed a general-purpose diffractometer at BL02B1 for structure analysis. The first data, taken for five days, gave satisfactory results to evaluate the system. The powder diffraction equipment, the vacuum camera and the seven-axis diffractometer are well designed and constructed. The beamline will be opened to the public at the beginning of October 1997.

We would like to acknowledge Mr Shobu, Dr Kuroiwa, Dr Ozawa, Dr Kubota and Dr Yamamoto for help in carrying out the first experiments at BL02B1. The Pt–Ni chain sample was made available by Dr Yamashita of Nagoya University.

References

- Kuroiwa, Y., Tamura, I., Ohe, F., Jidaisho, H., Akiyama, K. & Noda, Y. (1995). *J. Appl. Cryst.* **28**, 341–346.
- Noda, Y., Kuroiwa, Y., Konishi, H., Sakaue, K. & Terauchi, H. (1996). *SPring-8 Annual Report*, pp. 86–87. SPring-8, Hyogo 678–12, Japan.